Comparison of Two Techniques for Radiofrequency Hepatic Tumor Ablation through Numerical Simulation

N. Kosturski, S. Margenov, and Y. Vutov

Citation: AIP Conf. Proc. **1404**, 431 (2011); doi: 10.1063/1.3659945
View online: http://dx.doi.org/10.1063/1.3659945
View Table of Contents: http://proceedings.aip.org/dbt/dbt.jsp?KEY=APCPCS&Volume=1404&Issue=1
Published by the American Institute of Physics.

Comparison of Two Techniques for Radio-frequency Hepatic Tumor Ablation through Numerical Simulation

N. Kosturski, S. Margenov and Y. Vutov

Institute of Information and Communication Technologies, BAS, Acad. G. Bonchev str., bl. 25A, 1113 Sofia, Bulgaria

Abstract. We simulate the thermal and electrical processes, involved in the radio-frequency ablation procedure. In this study, we take into account the observed fact, that the electrical conductivity of the hepatic tissue varies during the procedure. With the increase of the tissue temperature to a certain level, a sudden drop of the electrical conductivity is observed. This variation was neglected in some previous studies.

The mathematical model consists of two parts – electrical and thermal. The energy from the applied AC voltage is determined first, by solving the Laplace equation to find the potential distribution. After that, the electric field intensity and the current density are directly calculated. Finally, the heat transfer equation is solved to determine the temperature distribution. Heat loss due to blood perfusion is also accounted for.

The simulations were performed on the IBM Blue Gene/P massively parallel computer.

Keywords: Radio-frequency ablation, Bio-heat equation, FEM, PCG
PACS: 02.60.Cb, 02.60.Dc, 02.60.Lj, 02.70.Dh

INTRODUCTION

The liver is a common location of tumors. Not all patients are suitable for surgical tumor removal. Alternative techniques for treating such patients are sought. One such technique is the radio-frequency (RF) ablation. It is a low invasive technique for the treatment of hepatic tumors, utilizing AC current to destroy the tumor cells by heating ([6, 7]). The RF ablation procedure destroys the unwanted tissue by heating, arising when the energy dissipated by the electric current flowing through a conductor is converted to heat. The destruction of the cells occurs at temperatures of 45°C–50°C. The procedure is relatively safe, as it does not require open surgery.

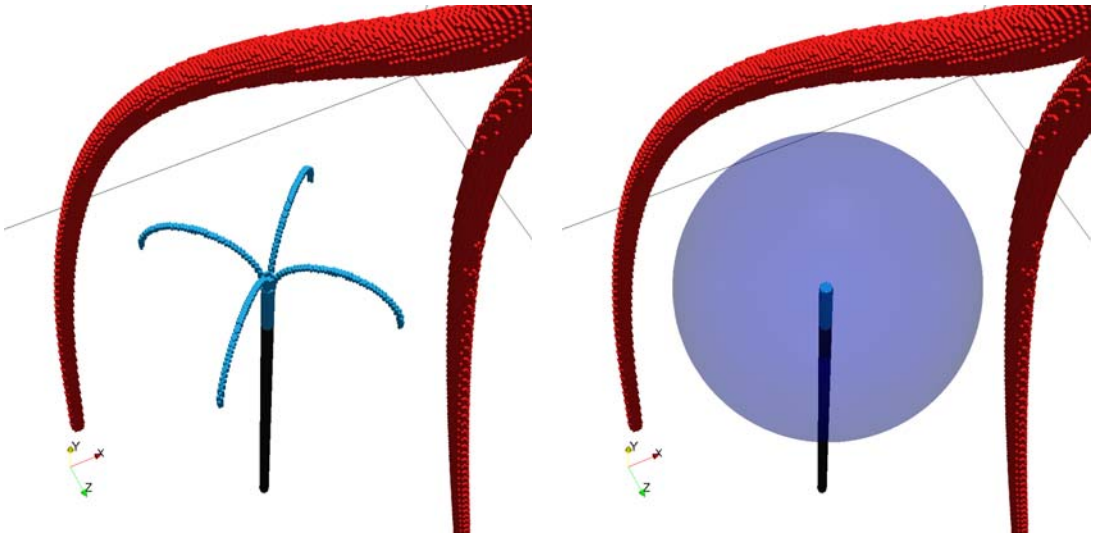

FIGURE 1. The structures of the two considered RF probes

An electrical probe is inserted in the liver. Here, we compare two different RF probe designs (illustrated on

Application of Mathematics in Technical and Natural Sciences
AIP Conf. Proc. 1404, 431-437 (2011); doi: 10.1063/1.3659945

Figure 1). The first one (on the left) consists of a stainless steel trocar with four nickel-titanium retractable electrodes. Polyurethane is used to insulate the trocar. The RF ablation procedure starts by placing the straight RF probe inside the tumor. The surgeon performs this under computer tomography (CT) or ultrasound guidance. Once the probe is in place, the electrodes are deployed and RF current is initiated. Both the surfaces areas of the uninsulated part of the trocar and the electrodes conduct RF current.

The second RF probe design (on the right) has no retractable electrodes. Saline solution in injected through the needle with a constant pressure during the procedure instead, increasing the electrical conductivity of the saturated tissue. Some additional complexity is associated with this design, arising from the flow of the injected fluid and it's effects on the electrical and thermal processes. We are currently at an early stage of developing our model. We considers a spherical bubble centered around the tip of the needle to be saturated with saline solution throughout the whole procedure. The electrical conductivity of the saturated tissue is 50 % higher than that of the normal tissue.

THE MATHEMATICAL MODEL

The RF ablation procedure destroys the unwanted tissue by heating, arising when the energy dissipated by the electric current flowing through a conductor is converted to heat. The bio-heat time-dependent partial differential equation [6, 7]

$$\rho c \frac{\partial T}{\partial t} = \nabla \cdot k \nabla T + J \cdot E - h_{bl}(T - T_{bl}) \tag{1}$$

is used to model the heating process during the RF ablation. The term $J \cdot E$ in (1) represents the thermal energy arising from the current flow and the term $h_{bl}(T - T_{bl})$ accounts for the heat loss due to blood perfusion.

The following initial and boundary conditions are applied

$$\begin{aligned} T &= 37^{\circ}\text{C when } t = 0 \text{ at } \Omega, \\ T &= 37^{\circ}\text{C when } t \geq 0 \text{ at } \partial\Omega. \end{aligned} \tag{2}$$

The following notations are used in (1) and (2):

- Ω – the entire domain of the model;
- $\partial\Omega$ – the boundary of the domain;
- ρ – density (kg/m^3);
- c – specific heat (J/kg K);
- k – thermal conductivity (W/m K);
- J – current density (A/m);
- E – electric field intensity (V/m);
- t – time (s);
- T – temperature (C);
- T_{bl} – blood temperature (37°C);
- w_{bl} – blood perfusion (1/s);
- $h_{bl} = \rho_{bl} c_{bl} w_{bl}$ – convective heat transfer coefficient accounting for the blood perfusion in the model.

The bio-heat problem is solved in two steps. The first step is finding the potential distribution V of the current flow. With both considered RF probe design, the current is flowing from the conducting electrodes to a dispersive electrode on the patient's body. The electrical flow is modeled by the Laplace equation

$$\nabla \cdot \sigma \nabla V = 0, \tag{3}$$

with boundary conditions

$$\begin{aligned} V &= 0 \text{ at } \partial\Omega, \\ V &= V_0 \text{ at } \partial\Omega_{el}. \end{aligned}$$

The following notations are used in the above equations:

- V – potential distribution in Ω;
- σ – electric conductivity (S/m);
- V_0 – applied RF voltage;
- $\partial\Omega_{el}$ – surface of the conducting part of the RF probe.

After determining the potential distribution, the electric field intensity and the current density can be computed from

$$E = -\nabla V, \qquad J = \sigma E.$$

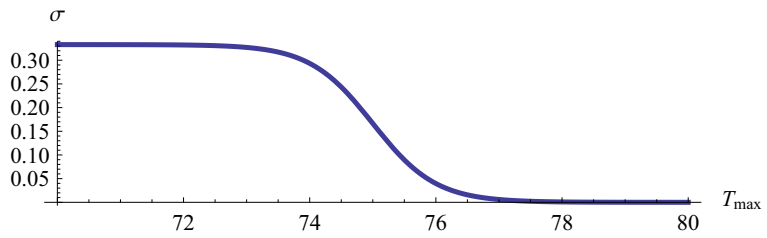

FIGURE 2. Variation of the electrical conductivity: $\sigma(\mathbf{x})$, $\sigma_{max} = 0.333$, $\sigma_{min} = 10^{-5}$

For the purpose of comparing the two probes, as well as following more closely the actual medical equipment, we need to determine the potential V_0 for the second boundary condition of (3) that will yield a certain electrical power P. To do this, the Laplace equation is initially solved with an arbitrary boundary condition $V = V_0^*$ at $\partial\Omega_{el}$. Then, E^* and J^* are obtained from the solution and the corresponding electrical power P^* can be computed as

$$P^* = \int_\Omega E^* \cdot J^* d\mathbf{x}.$$

Since the solution and all the components of E and J are proportional to the value of V_0 we can scale the obtained solution, instead of recomputing it, in the following way

$$V_0 = \lambda V_0^*, \quad E = \lambda E^*, \quad J = \lambda J^*, \quad \text{where} \quad \lambda = \sqrt{P/P^*}.$$

Let us note that this adjustment is performed only once in the beginning of the simulation. The obtained potential V_0 remains constant during the RF ablation procedure.

In this study, we consider an enhancement to the model, following the observation that the electrical conductivity of the tissue suddenly drops after reaching a certain temperature. We performed some experiments with the second probe type on a fresh pork liver. The RF equipment was constantly monitoring the electrical current. In the case, when saline solution was not injected in the tissue, we observed a sudden increase in the electrical resistance and a corresponding drop in the electrical power. This happened just a few seconds after the start of the procedure and is explained by overheating of the tissue around the electrode. The exact tissue temperature could not be measured, but we currently believe this effect to occur at 70°C–80°C. To model this behavior we chose the function

$$\sigma(\mathbf{x}) = \frac{1}{2}\left(\sigma_{max} + \sigma_{min} + (\sigma_{max} - \sigma_{max})\tanh(75 - T_{max}(\mathbf{x}))\right) \tag{4}$$

to associate the electrical conductivity σ of the liver tissue with the maximum temperature reached T_{max} (see Figure 2).

We solve the heat transfer equation (1) using the heat source $J \cdot E$.

NUMERICAL SIMULATION

For the numerical solution of both of the above discussed steps of the simulation the Finite Element Method (FEM) in space is used ([2]). Linear conforming elements are chosen in this study. They provide a simple implementation in combination with a guaranteed optimal convergence rate and parallel scalability of the applied algebraic multigrid (AMG) preconditioner. To apply the linear FEM discretization to the voxel domain, each voxel is split into six tetrahedra. To solve the bio-heat equation, after the space discretization, the time derivative is discretized via finite differences and the backward Euler scheme is used ([3]).

Let us denote with K^* the stiffness matrix coming from the FEM discretization of the Laplace equation (3). It can be written in the form

$$K^* = \left[\int_\Omega \sigma \nabla\Phi_i \cdot \nabla\Phi_j d\mathbf{x}\right]_{i,j=1}^{N},$$

where $\{\Phi_i\}_{i=1}^N$ are the FEM basis functions.

The system of linear algebraic equations

$$K^* X = 0 \tag{5}$$

is to be solved to find the nodal values X of the potential distribution.

The electric field intensity and the current density are than expressed by the partial derivatives of the potential distribution in each finite element. This way, the nodal values F for the thermal energy $E \cdot J$ arising from the current flow are obtained.

Let us now turn our attention to the discrete formulation of the bio-heat equation. Let us denote with K and M the stiffness and mass matrices from the finite element discretization of (1). They can be written as

$$K = \left[\int_{\Omega} k \nabla \Phi_i \cdot \nabla \Phi_j d\mathbf{x} \right]_{i,j=1}^{N},$$

$$M = \left[\int_{\Omega} \rho c \Phi_i \Phi_j d\mathbf{x} \right]_{i,j=1}^{N}.$$

Let us also denote with Ω_{bl} the subdomain of Ω occupied by blood vessels and with M_{bl} the matrix

$$M_{bl} = \left[\int_{\Omega} \delta_{bl} h_{bl} \Phi_i \Phi_j d\mathbf{x} \right]_{i,j=1}^{N},$$

where

$$\delta_{bl}(x) = \begin{cases} 1 \text{ for } x \in \Omega_{bl}, \\ 0 \text{ for } x \in \Omega \setminus \Omega_{bl}. \end{cases}$$

Than, the parabolic equation (1) can be written in matrix form as:

$$M \frac{\partial T}{\partial t} + (K + M_{bl}) T = F + M_{bl} T_{bl}. \tag{6}$$

If we denote with τ the time-step, with T^{n+1} the solution at the current time level, and with T^n the solution at the previous time level and approximate the time derivative in (6) we obtain the following system of linear algebraic equations for the nodal values of T^{n+1}

$$A T^{n+1} = M T^n + \tau G, \tag{7}$$

where

$$A = M + \tau (K + M_{bl}) \quad \text{and} \quad G = F + M_{bl} T_{bl}.$$

A vector, containing the nodal values T_{max} of the maximum temperature in time, is updated on each time-step. After that, the electrical conductivity coefficients are varied according to (4) in the region of the domain representing the liver tissue. Than, the Laplace equation (3) is discretized and solved again to reflect any eventual changes in the electrical power and the corresponding heat source.

The matrices K^* and A of the linear systems (5) and (7) are ill-conditioned and very large, having around 10^8 rows. Since they are symmetric and positive definite, we use the PCG [1] method, which is the most efficient solution method in this case.

A parallel AMG implementation – BoomerAMG [4, 8] is used to precondition the linear systems. Since the matrix A is not varied between time steps, we only construct the algebraic multigrid, corresponding to it, once, before the first time-step. It can be readily used after that to precondition the linear systems for all subsequent time steps. The preconditioner corresponding to the matrix K^* is also reused on each time-step, although the matrix itself is varied. We reconstruct the AMG only when the number of PCG iterations reaches a certain limit, but it turned out to be rarely, if ever, necessary. The number of PCG iterations remained stable most of the time, despite the matrix variation. Additional details concerning our parallelization approach can be found in our paper [5].

TABLE 1. Thermal and electrical properties of the materials

Material	ρ **(kg/m^3)**	c **(J/kg K)**	k **(W/m K)**	σ **(S/m)**
Ni-Ti	6 450	840	18	10^8
Stainless steel	7 013	405	71	4×10^8
Liver	1 060	3 600	0.512	0.333
Saturated zone	1 030	3 890	0.528	0.5
Blood	1 000	4 180	0.543	0.667
Polyurethane	70	1 045	0.026	10^{-5}

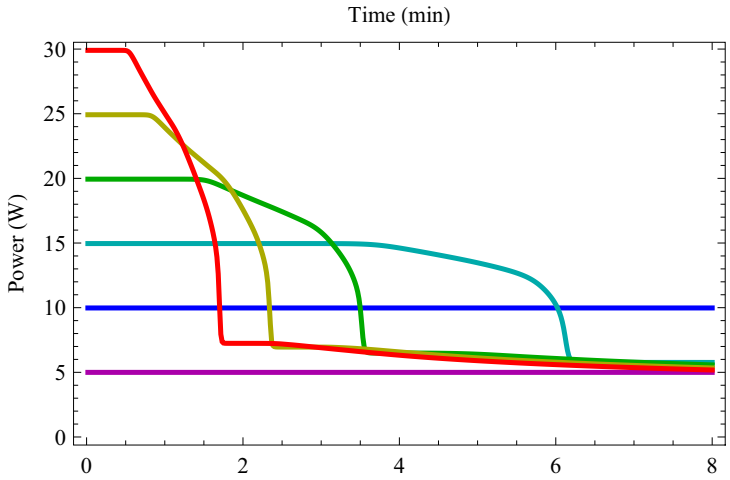

FIGURE 3. Electrical power over time

NUMERICAL SIMULATION RESULTS

The results presented in this section are based on a high-resolution ($512 \times 512 \times 512$) voxel-based representation of the computational domain. The domain consists of liver and tumor tissues, a large bifurcated blood vessel and the RF ablation probe (see Figure 1). In the case of the second considered probe design it also contains a bubble of the tissue, saturated with saline solution.

Table 1 lists the thermal and electrical properties of the materials, most of which are taken from [6] as well as the blood perfusion coefficient $w_{bl} = 6.4 \times 10^{-3}$ 1/s.

Four variants of the simulation were performed – two for each considered RF probe design. For the first type of probe we have performed two simulations – with and without taking into account the variation of the electrical conductivity. For the second RF probe, we simulated a dry process, to confirm it models well the experimentally observed effect. We also simulated the process when saline solution is injected. Simulations for each variant were performed using six different settings for the initial electrical power (5 W, 10 W, 15 W, 20 W, 25 W, and 30 W). The duration of the RF ablation procedure was 8 minutes, and a time-step of $\tau = 1$ s was used.

Simulations for the second probe design, without injecting saline solution, indeed confirmed our observations as the power quickly dropped to zero and the ablation process stopped. We, therefore, studied the effect of this model enhancement on the first probe design. The electrical power during the ablation process is presented in Figure 3. Although the power does not drop to 0 in this case, a steep drop is present. Our numerical results show that the drop appears after a shorter duration, when higher initial electrical power is applied.

The next results, show the effect of the drop on the outcome of the RF ablation procedure. The volume of the tissue, that reached or exceeded 50°C was computed during the simulation and is presented in Figure 4. This results clearly indicate that higher power does not always correspond to a larger volume being ablated. For example, starting with 15 W of electrical power, the ablated volume after 5 minutes was larger, than the volume with 30 W in 8 minutes.

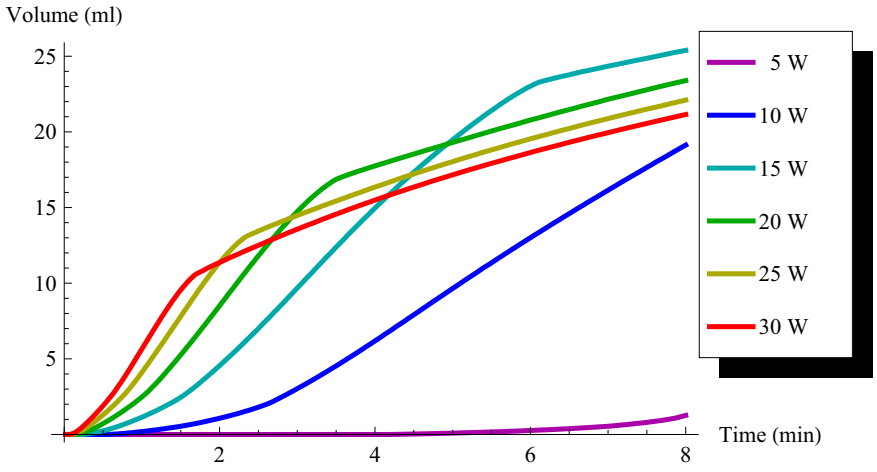

FIGURE 4. Ablated region volume in time

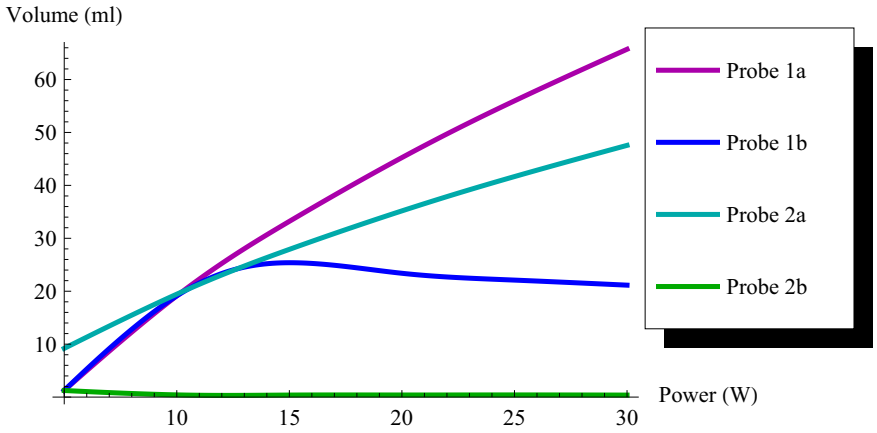

FIGURE 5. Electrical power correspondence to ablated volume

Finally, to compare the two considered designs, we show the relation between the initial electrical power and the volume of ablated tissue in all four considered cases in Figure 5. Probe 1a corresponds to the case, where the variation in conductivity is neglected. It is taken into account for Probe 1b. It is clearly visible that the variation has a significant impact when high power is applied. Probe 2a corresponds to the case when saline solution is injected and 2b – to a dry process. The ablated volume with the dry process is very small, exactly as expected. However, the results when saline solution is injected show some possible advantage of the second RF probe design. The typical shapes of the ablated regions for the two probe designs are shown in Figure 6. The second design leads to a much simpler oval shape, which is arguably another possible advantage, as it may be simpler to predict when the whole tumor is ablated.

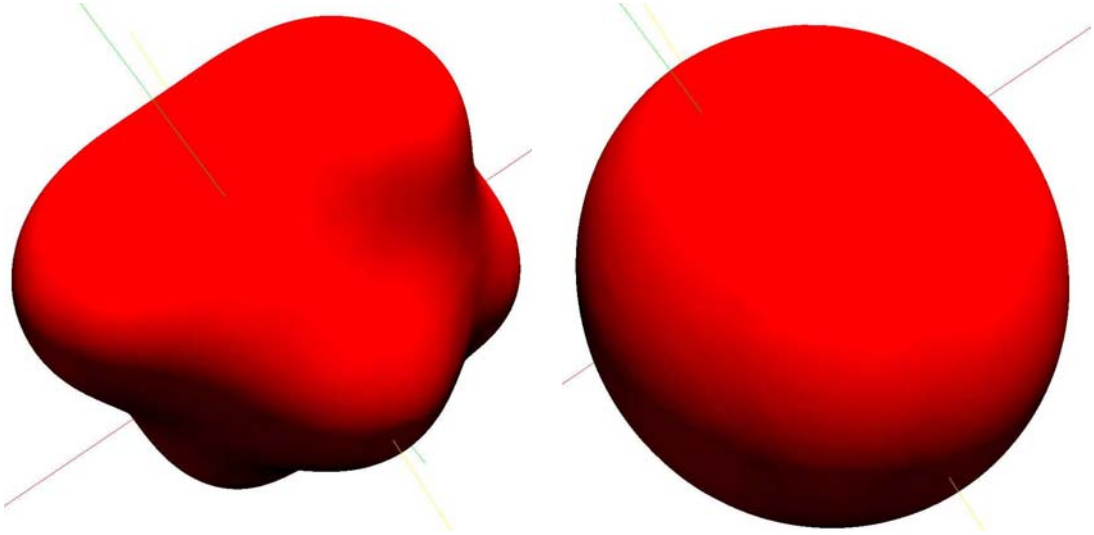

FIGURE 6. Typical shapes of the ablated region for the considered probes

CONCLUDING REMARKS

Two RF ablation probe designs are compared through numerical simulation. An enhancement of the model of the processes in the RF ablation procedure is presented, following some experimental observations using the second design. It's effect on the first design is studied and the results indicate that it is significant.

We plan to enhance the model for the second considered probe design, taking into account the actual flow.

ACKNOWLEDGMENTS

This work is partly supported by the Bulgarian NSF Grants DCVP 02/1 and DPRP7RP02/13. We would like to thank Theodor Popov (AMET Ltd.) for providing the RF ablation equipment as well as many valuable insights. We also kindly acknowledge the support of the Bulgarian Supercomputing Center for the access to the IBM Blue Gene/P supercomputer.

REFERENCES

1. O. Axelsson, *Iterative Solution Methods*, Cambridge University Press, 1996.
2. S. Brenner and L. Scott, *The mathematical theory of finite element methods*, Texts in applied mathematics, **15**, Springer-Verlag, 1994.
3. E. Hairer, S.P. Norsett, and G. Wanner *Solving ordinary differential equations I, II*, Springer Series in Comp. Math., 2000, 2002
4. V.E. Henson and U.M. Yang (2002) BoomerAMG: A parallel algebraic multigrid solver and preconditioner, *Applied Numerical Mathematics* **41**(1), Elsevier, 155–177.
5. N. Kosturski, S. Margenov, and Y. Vutov, "Improving the Efficiency of Parallel FEM Simulations on Voxel Domains," in *Proceedings of LSSC'11*, to appear as a special volume of *Lecture Notes in Computer Science*.
6. S. Tungjitkusolmun, S.T. Staelin, D. Haemmerich, J.Z. Tsai, H. Cao, J.G. Webster, F.T. Lee, D.M. Mahvi, and V.R. Vorperian (2002) Three-dimensional finite-element analyses for radio-frequency hepatic tumor ablation, *IEEE transactions on biomedical engineering* **49**(1), 3–9.
7. S. Tungjitkusolmun, E.J. Woo, H. Cao, J.Z. Tsai, V.R. Vorperian, and J.G. Webster (2000) Thermal-electrical finite element modelling for radio frequency cardiac ablation: Effects of changes in myocardial properties, *Medical and Biological Engineering and Computing* **38**(5), 562–568.
8. Lawrence Livermore National Laboratory, *Scalable Linear Solvers Project*, URL: `http://www.llnl.gov/CASC/linear_solvers/`.